Monthly Notices
of the
ROYAL ASTRONOMICAL SOCIETY

Mon. Not. R. Astron. Soc. **401,** 933–940 (2010) doi:10.1111/j.1365-2966.2009.15728.x

High-redshift elliptical galaxies: are they (all) really compact?

C. Mancini,[1⋆] E. Daddi,[2] A. Renzini,[1] F. Salmi,[2] H. J. McCracken,[3] A. Cimatti,[4] M. Onodera,[2] M. Salvato,[5] A. M. Koekemoer,[6] H. Aussel,[2] E. Le Floc'h,[2,7] C. Willott[8] and P. Capak[9,10]

[1]*Osservatorio Astronomico di Padova (INAF-OAPD), Vicolo dell'Osservatorio 5, I-35122 Padova, Italy*
[2]*CEA-Saclay, DSM/DAPNIA/Service d'Astrophysique, 91191 Gif-Sur Yvette Cedex, France*
[3]*Institut d'Astrophysique de Paris, UMR7095, Université Pierre et Marie Curie, 98 bis Boulevard Arago, 75014 Paris, France*
[4]*Dipartimento di Astronomia, Università di Bologna, via Ranzani 1, I-40127 Bologna, Italy*
[5]*California Institute of Technology, 105-24 Robinson, 1200 E. California Blvd., Pasadena, CA 91125, USA*
[6]*Space Telescope Science Institute, 3700 San Martin Drive, Baltimore, MD 21218, USA*
[7]*Institute for Astronomy, University of Hawaii, 2680 Woodlawn Drive, Honolulu, HI 96822, USA*
[8]*Herzberg Institute of Astrophysics, National Research Council, 5071 West Saanich Rd, Victoria, BC V9E 2E7, Canada*
[9]*Spitzer Science Center, 314-6 Caltech, Pasadena, CA 91125, USA*
[10]*California Institute of Technology, MS 104-25 Pasadena, CA 91125, USA*

Accepted 2009 September 16. Received 2009 September 7; in original form 2009 July 10

ABSTRACT

We investigate the properties of 12 ultramassive passively evolving early-type galaxies (ETGs) at $z_{\rm phot} > 1.4$ in the COSMOS 2 deg^2 field. These 12 ETGs were selected as *pBzK*s, have accurate $1.4 \lesssim z_{\rm phot} \lesssim 1.7$, high Sérsic index profiles typical of ellipticals, no detection at 24 μm, resulting in a complete ETG sample at $M* > 2.5 \times 10^{11}\,{\rm M}_{\odot}$ (Chabrier initial mass function). Contrary to the previous claims, the half-light radii estimated in very high signal-to-noise ratio imaging data from *Hubble Space Telescope*+Advanced Camera for Surveys (ACS) are found to be large for most of the sample, consistent with local ellipticals. If the high-redshift ETGs with $M* < 2.5 \times 10^{11}\,{\rm M}_{\odot}$ are really small in size and compact as reported in the previous studies, our result may suggest a 'downsizing' scenario, whereby the most massive ETGs reach their final structure earlier and faster than the lower mass ones. However, simulating galaxies with morphological properties fixed to those of local ETGs with the same stellar mass show that the few compact galaxies that we still recover in our sample can be understood in terms of fluctuations due to noise preventing the recovery of the extended low surface brightness haloes in the light profile. Such haloes, typical of Sérsic profiles, extending even up to 40 kpc, are indeed seen in our sample.

Key words: galaxies: evolution – galaxies: formation – galaxies: elliptical and lenticular, cD – galaxies: high-redshift.

1 INTRODUCTION

Understanding the formation processes of galactic spheroids, i.e. bulges and early-type galaxies (ETGs), remains a central theme in the context of galaxy formation and evolution. The discovery of a widespread population of passively evolving ETGs at $z > 1.4$ proved that quenching of star formation in massive galaxies is well under way by $z \sim 2$ (Cimatti et al. 2004; Glazebrook et al. 2004).

Further studies of high-redshift ETGs then revealed an unexpected property of a sizable fraction of them: many such ETGs appear to have much smaller effective radii ($R_{\rm e}$; by factors of ∼2 to ∼4) with respect to ETGs of comparable stellar mass ($M*$) in the local Universe (Daddi et al. 2005, hereafter D05), a result then confirmed by several other studies (e.g. Trujillo et al. 2006, 2007; Longhetti et al. 2007; Toft et al. 2007; Zirm et al. 2007; Buitrago et al. 2008; Cimatti et al. 2008; McGrath et al. 2008; Rettura et al. 2008; van Dokkum et al. 2008; Damjanov et al. 2009; Saracco, Longhetti & Andreon 2009). ETGs with similar stellar densities appear to be extremely rare in the local Universe (Trujillo et al. 2009; Taylor et al. 2009; but see Valentinuzzi et al. 2009), although it has been argued that such compact high-redshift ETGs have survived as the cores of the present-day massive spheroids (Hopkins et al. 2009).

It has also been argued that the $R_{\rm e}$–$M*$ relation for ETGs would keep evolving also from $z \sim 1$ all the way to $z \sim 0$, with a steady increase of $R_{\rm e}$ for given $M*$ (van der Wel et al. 2008; Bernardi 2009; Maier et al. 2009).

The formation of very compact ETGs at high redshift may not be a problem: submillimetre galaxies appear to have comparable masses

⋆E-mail: chiara.mancini@oapd.inaf.it

(largely in gas form) and radii, hence may likely be precursors to compact ETGs (Cimatti et al. 2008; Tacconi et al. 2008), turning into them upon expulsion of their residual gas. However, no generally accepted explanation has yet been established on how such compact ETGs would evolve into their present descendants, i.e. how they can inflate to reach two to four times larger effective radii.

ETG–ETG (dry) merging soon appeared to be a plausible mechanism (e.g. Khochfar & Silk 2006), but most such events would result in an increase of both mass and radius such as to move galaxies parallel to the local R_e–$M*$ relation, rather than towards it (Cimatti et al. 2008; Saracco et al. 2009). Moreover, major dry merging events may be too rare anyway, as the vast majority of high-z ETGs do not appear to have close ETG companions of similar brightness (Cimatti et al. 2008). Having excluded major mergers, accretion of many satellites (i.e. minor dry mergers) was then considered, either adding an extended envelope to the compact core (Cimatti et al. 2008) or expanding such core by heating gravitationally (Naab et al. 2007). It has also been suggested that the expansion of high-z ETGs would be the result of active galactic nuclei (AGN) feedback driving the rapid expulsion of the residual gas (Fan et al. 2008), but such expansion must take place in at most a few dynamical times ($\sim 10^8$ yr), hence only very few objects could be caught as already passive and still compact.

On the other hand, the possibility that the apparent small radii may not be real was not completely excluded. This could be either the effect of part of the light coming from a centrally concentrated source (e.g. an AGN or central starburst) or to some systematic bias not having been taken into full account (D05; Pannella, Gabasch & Goranova 2009). Recently, La Barbera et al. (2009) have argued for the presence of a radial age gradient in local ETGs, that would result in an apparent decrease of R_e with increasing redshift, as the younger, more centrally concentrated population differentially brightens w.r.t. the older and broader stellar component. However, there appears to be no strong colour gradients in the few cases in which both optical and near-infrared (IR) *Hubble Space Telescope* (*HST*) imaging is available for high-z ETGs (e.g. Toft et al. 2007), or within different ACS bands (D05). In this paper, we present the results of two-dimensional (2D) surface brightness profile fitting of a complete sample of 12 extremely massive ETGs ($M* > 2.5 \times 10^{11}\,M_\odot$) at $z \gtrsim 1.4$, using the *HST*+ACS/Wide Field Camera (WFC) images of the COSMOS 2 deg^2 field (Koekemoer et al. 2007). Selection of high-z ETGs over such a large area allows us to pick the most massive/luminous high-z ETGs and tackle the size issue with the highest signal-to-noise ratio (S/N).

2 DATA, SAMPLE SELECTION AND SED FITTING

A sample of extremely massive ETGs was extracted from the catalogue of K-selected galaxies in the 2 deg^2 COSMOS field (McCracken et al. 2009). From this catalogue, we extracted all the objects with K_s(Vega) < 17.7, whose corresponding BzK plot is shown in Fig. 1. From this sample, we then selected the brightest galaxies satisfying the passive BzK-galaxy criterion of Daddi et al. (2004), for which the K_s(Vega) < 17.7 limit roughly corresponds to $M* > 2.5 \times 10^{11}\,M_\odot$ at $z \sim 1.5$ for a Chabrier initial mass function (IMF). This resulted in a sample of 22 sources, having retained only galaxies with IRAC 3.6 μm detections with separations <0.6 arcsec from the K-band positions, a criterion required to avoid objects affected by blending in the Infra-Red Array Camera (IRAC) and Multi-band Imaging Photometer for *Spitzer* (MIPS) images (see e.g. Daddi et al. 2007). We note that four star-forming BzK galaxies

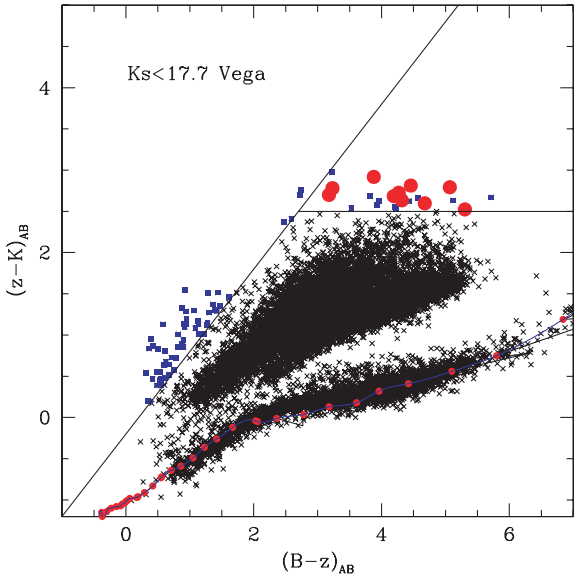

Figure 1. The BzK two-colour diagram for all objects with $K_s < 17.7$ (Vega system) in the COSMOS field. The 12 bona fide passive ETGs are shown as red circles. Blue squares with $(z - K) < 1.6$ are most likely AGN-dominated galaxies, having point-like morphology and/or X-ray emission. The remaining blue squares with redder $(z - K)$ colours show $sBzK$ galaxies and $pBzK$ contaminants rejected for being star-forming. The blue solid line and the red dots in the bottom show the expected colours for the stars (from Lejeune, Cuisinier & Buser 1997), overlapping with the locus of real star sequences.

($sBzK$) are found to $K < 17.7$, after excluding likely AGNs among $sBzK$s, i.e. the blue squares with $(z - K) < 1.6$ in Fig. 1. The colours of these four objects are close to the $pBzK$ boundary, and in principle some genuine ETG could have been scattered there just by photometric errors noise. However, we find that all four objects are well detected at 24 μm.

Since these 22 $pBzK$-selected objects could include heavily dust-reddened star-forming galaxies at $z < 1.4$, we carefully checked the properties of the sample to solidly identify the bona fide ETGs and discard possible contaminants. We requested all of the following criteria for retaining ETG candidates:

(i) non-detection at 24 μm in the *Spitzer*+MIPS data (Sanders et al. 2007). We used the most recent deep catalogue by Aussel & Le Floc'h, reaching 5σ completeness levels down to 80 μJy (Le Floc'h et al. 2009). This corresponds to a limit of star formation rate (SFR) $< 50\,M_\odot\ \mathrm{yr}^{-1}$ for $z \sim 1.5$, using the models of Chary & Elbaz (2001);

(ii) elliptical-like compact morphology, based on a visual inspection of the ACS I-band images (Fig. 2);

(iii) multicolour SEDs best fitted with old, passively evolving populations with no dust reddening as shown in Fig. 3. SEDs were constructed using COSMOS photometry in the B-, i-, z-, J-, K-band data consistently with McCracken et al. (2009), expanded to include photometry in the first three IRAC bands (from Ilbert, Salvato and S-COSMOS collaboration; Ilbert et al. 2009).

We found that 12 of the 22 $pBzK$ galaxies do satisfy all these criteria and are retained as our sample of bona fide $z \gtrsim 1.4$ ETGs. The remaining 10 galaxies that were discarded are found to fail multiple criteria in most cases: they tend to be 24 μm detected (6/10), have irregular (or point-like, unresolved) morphologies in

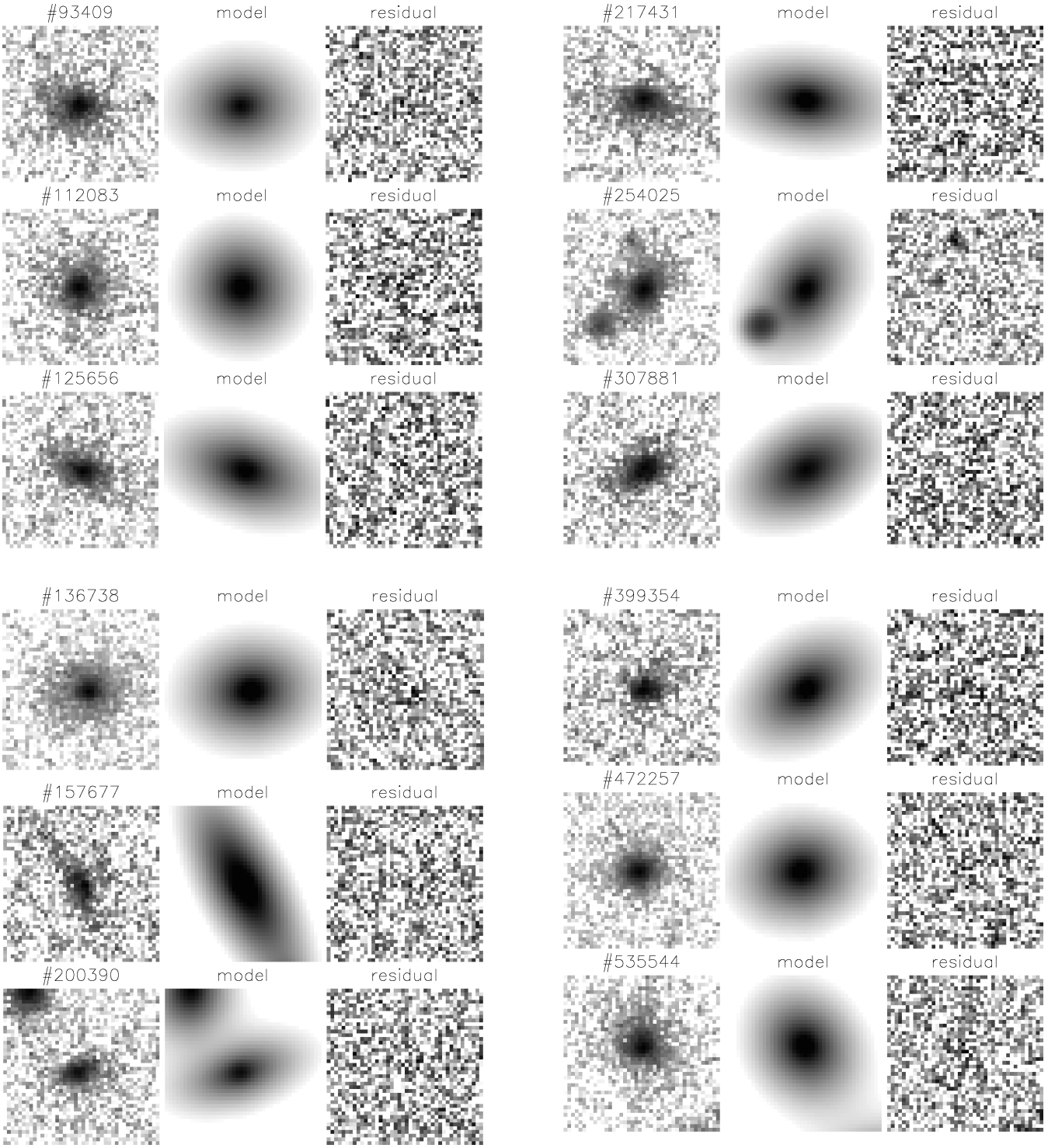

Figure 2. ACS *I*-band 2.5 arcsec cutouts for the 12 bona fide ETGs, their best-fitting models and the corresponding residuals. Images are displayed in logarithmic scale to enhance low surface brightness details.

the ACS imaging (7/10), are best fitted by star-forming galaxy templates with large amounts of reddening (7/10) or show evidence for strong AGN contamination of the optical/near-IR light (3/10) as indicated by the 'power-law' shape of the SED and X-ray and/or radio detection. These criteria are very efficient in selecting truly passively evolving ETGs, as confirmed by their spectroscopic identification in the Hubble Ultra Deep Field (HUDF) by D05.

Photometric redshifts and stellar masses were derived from the SEDs using the HYPERZ code (Bolzonella, Miralles & Pelló 2000), and fitting photometric data with simple stellar populations (SSP) as well as with composite populations described by τ-models (SFR $\propto e^{-t/\tau}$, with $\tau =$ from 0.1 Gyr to ∞), and using the population models of Maraston (2005). This parametrization of the star formation history may be inappropriate for actively star-forming

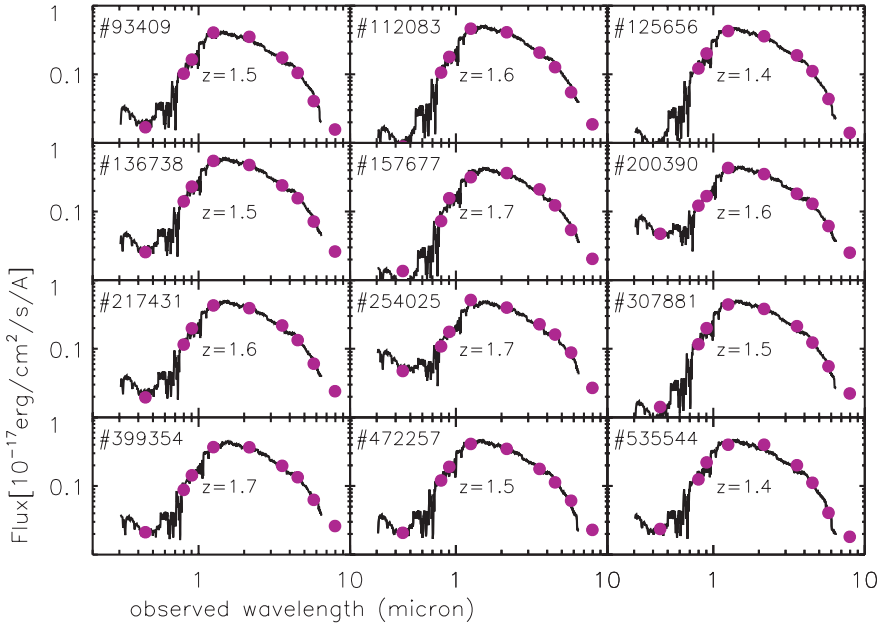

Figure 3. Multicolour SED and best-fitting SED templates (Maraston 2005; Chabrier IMF) of the 12 bona fide ETGs.

Table 1. Characteristics of the final sample of 12 ETGs.

ID	RA (J200)	Dec. (J200)	m_{814}	R_e (arcsec)	R_e (kpc)	n	z_{ph}	log(M*)	Age	A_V	K_s
93409	10:01:27.0044	01:39:53.1198	22.73 ± 0.08	0.78 ± 0.11	6.70 ± 0.92	4.26 ± 0.34	1.52	11.45	2.40	0.08	17.68
112083	09:59:11.4551	01:42:25.2173	22.93 ± 0.05	0.44 ± 0.04	3.73 ± 0.32	3.33 ± 0.21	1.61	11.63	2.75	0.00	17.51
125656	10:00:22.9577	01:44:16.8353	22.53 ± 0.07	0.73 ± 0.09	6.26 ± 0.81	4.37 ± 0.35	1.43	11.48	2.75	0.08	17.66
136738	09:59:47.0280	01:45:52.2360	21.98 ± 0.11	2.02 ± 0.45	17.27 ± 3.84	7.29 ± 0.58	1.59	11.64	2.40	0.00	17.35
157677	10:01:34.2920	01:48:32.0022	22.51 ± 0.20	3.20 ± 1.06	27.36 ± 9.03	4.46 ± 0.62	1.70	11.58	2.50	0.00	17.64
200390	10:01:01.9974	01:54:32.4251	23.43 ± 0.11	0.68 ± 0.14	5.81 ± 1.24	4.57 ± 0.60	1.61	11.47	2.00	0.08	17.68
217431	10:02:39.5288	01:56:59.1162	21.85 ± 0.12	2.22 ± 0.47	18.92 ± 3.98	4.81 ± 0.44	1.61	11.57	2.40	0.00	17.56
254025	10:02:28.4912	02:02:13.6899	22.50 ± 0.06	0.68 ± 0.07	5.79 ± 0.61	4.14 ± 0.26	1.71	11.64	2.10	0.08	17.54
307881	10:02:35.6396	02:09:14.3640	22.95 ± 0.04	0.37 ± 0.02	3.16 ± 0.20	1.92 ± 0.12	1.52	11.53	2.50	0.08	17.59
399354	10:02:49.4055	02:21:47.4012	22.98 ± 0.14	0.75 ± 0.20	6.39 ± 1.60	4.57 ± 0.64	1.70	11.59	2.30	0.08	17.63
472257	10:01:06.0754	02:31:35.1966	23.04 ± 0.04	0.25 ± 0.02	2.13 ± 0.14	3.63 ± 0.23	1.52	11.46	2.40	0.00	17.69
535544	10:00:00.6592	02:40:29.6220	22.29 ± 0.09	1.06 ± 0.16	9.03 ± 1.39	4.76 ± 0.35	1.41	11.41	2.30	0.16	17.54

Note. From left to right: ID: identification number in the catalogue of McCracken et al. (2009); RA (J2000) and Dec. (J2000): coordinates from WIRCAM/*K*-band data set; m_{814}: ACS F814W *I*-band magnitude; R_e: effective radius in arcsec and kpc; n: the Sérsic index; z_{ph}: photometric redshifts; log(M*): galaxy stellar masses in $M_\odot$ units; mean stellar age in Gyr; A_V reddening parameter; K_s : *K*-band WIRCAM+CHFT magnitude in Vega system.

galaxies (especially at high redshifts) because it assumes that all galaxies are caught at their minimum SFR. However, for passively evolving galaxies this assumption may not affect appreciably the redshift and mass determinations, as their SFR is indeed ∼0.

The 10 galaxies that we discarded as dusty contaminants are found to be at $z_{phot} < 1.4$. All 12 bona fide ETGs have photometric redshifts in the range of $1.4 < z_{phot} < 1.7$, are fitted by SSP models (Maraston 2005) older than ∼1 Gyr (i.e. with strong 4000Å/Balmer breaks) and have stellar masses in the range of $2.5 \times 10^{11} < M* < 4 \times 10^{11}\,M_\odot$, adopting the Chabrier (2003) IMF, as reported in Table 1. Following D05 and Maraston et al. (2006), we expect that photometric redshifts of ETGs computed in this way should be accurate to within $\Delta z \lesssim 0.1$.

3 SURFACE BRIGHTNESS PROFILE FITTING AND SIMULATIONS

We used GALFIT (Peng et al. 2002) to fit 2D Sérsic (1968) profiles to the *I*-band (F814W filter) ACS images of the 12 ETGs. The median integration over the COSMOS field is 2028 s, the pixel scale is ∼0.05 arcsec and the full width at half-maximum (FWHM) of the point spread function (PSF) is ∼0.097 arcsec. GALFIT was run on sky-subtracted images, obtained by the SEXTRACTOR software (Bertin & Arnouts 1996). Thus, the sky was fixed to a null value in the GALFIT procedure, and the galaxy Sérsic index (n), effective radius (R_e) and total magnitude (m_{814}) were left as free parameters. Other free parameters in the fit are the object position (x_c, y_c), the position angle of the major axis a and the axis ratio (b/a) between minor and major axes. On the other hand, leaving both n and the sky background as free parameters in GALFIT may lead to unreliable results for galaxies with intrinsically high values of n (see the GALFIT home page[1]). For each galaxy, the adopted PSF was obtained from the closest suitable bright unsaturated star. We verified that swapping PSF by using different stars in the COSMOS field or synthetic PSFs, built by means of the TINY TIM software package

[1] http://users.ociw.edu/peng/work/galfit/TFAQ.html#sensitivity

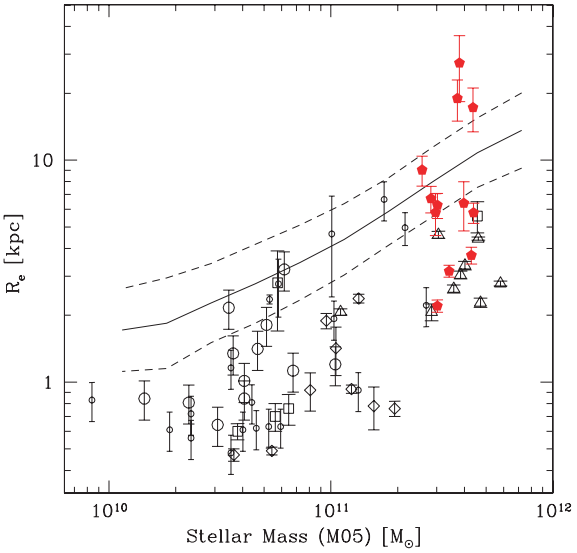

Figure 4. Mass versus size for ETGs at $z \geq 1.4$, compared with the local relation (solid line) and its 1σ dispersion (dashed lines). The figure is adapted from fig. 15 of Cimatti et al. (2008) by adding our 12 ETGs, shown as red large filled pentagons. Previous estimates of the effective radii of high redshift passive galaxies are shown as open symbols: big open circles are from Cimatti et al. (2008) (GMASS-CDFS); open triangles from Longhetti et al. (2007) and Trujillo et al. (2006); open squares are the HUDF passive BzK of D05 and Maraston et al. (2006); open diamonds show the sample of van Dokkum et al. (2008) after a mass-rescaling of a factor of ∼1.4, to Maraston (2005) models, for homogeneity with the other galaxies in the figure. The small open circles are from Zirm et al. (2007) (FIRES-HDFS), Toft et al. (2007) (FIRES- MS1054), McGrath et al. (2008) and Cimatti et al. (2004) (K20 survey). Credit: Cimatti et al., A&A, 482, 21, 2008, reproduced with permission © ESO.

(v. 6.3; see the TINY TIM User's Guide available online[2] by Krist & Hook 2004) gives virtually identical results. When galaxy isophotes partially overlap with bright close neighbours, we fitted galaxy and neighbours simultaneously (this was the case for objects 136738, 157677, 200390, 254025). For smaller and fainter neighbours, we used masked regions. Weight maps were used to account for shot noise and sky noise.

In Fig. 2, we show the galaxy ACS I-band images, the corresponding GALFIT best-fitting model and the residuals for each object. The best-fitting parameters m_{814}, the Sérsic index n (which measures the light central concentration) and the half-light radius R_e (i.e. circularized radius of the ellipse containing half of the total luminosity of the best-fitting Sérsic profile) are reported in Table 1. As shown in Fig. 4 and Table 1, only three of the 12 objects have very small effective radii for their mass ($0.25 < R_e < 0.48$ arcsec, i.e. ∼2 to ∼4 kpc at $z \sim 1.5$). This qualifies them as 'compact', compared to the local ellipticals, whereas the remaining nine objects appear to be consistent with local ETGs, although the effective radii of some of the objects with the largest size (e.g. 136738, 535544, 157677) also have very large intrinsic uncertainties. For all the objects but one we found $n > 3$, as expected for typical ETGs. The exception is object 307881, one of the smallest in the sample, which may consist of a bulge plus an exponential disc. On the contrary, the highest Sérsic index ($n = 7.29 \pm 0.58$) is found for object 136738. A large n generally indicates a highly centrally concentrated light profile, compatible with such massive elliptical galaxy. However, for this object the presence of some structure at the centre of the residual image (Fig. 2) suggests that a central unresolved point source (probably an AGN) may have contributed to increase the n value. Thus, we fitted object 136738 by adding a central point source, finding $R_e = 1.22$ arcs (∼10 kpc at $z = 1.6$), $n \sim 4$ and $m_{814} = 22.28$ for the Sérsic component, and a magnitude of $m_{814} = 25.88$ for the point-source component. We conclude that the possible presence of a point source would decrease by almost a factor of 2 of the resulting n value, but it would not dramatically affect the large $R_e(\geq 10$ kpc) found for this object, still consistent with the size of similarly massive local ETGs.

Fig. 4 shows that our 12 ETGs span a large range in size, although they have very similar masses. A large scatter in the size distribution was also found in other studies for less-massive galaxies. Note that the three smallest objects in our sample, with $R_e \lesssim 4$ kpc, are among the faintest in the full sample of 12 ETGs and are all fainter than $m_{814} = 22.9$. This leads us to wonder if the three small galaxies are really small as we have measured, or if their apparent small R_e is due to an observational bias. Thus, what we would like to clarify is whether the recovered distribution of n and R_e for our $z > 1.4$ ETG sample, including the three apparently small galaxies, could still be consistent with the local distribution of these structural parameters.

In order to answer this question, we have constructed a simulated set of galaxies all having $R_e = 7$ kpc and $n = 6$, which are the typical values for local ETGs with stellar masses as large as those estimated for the 12 ETG objects at $z > 1.4$ (Caon, Capaccioli & D'Onofrio 1993; Shen et al. 2003). The GALFIT package was used to generate synthetic galaxies with the chosen light profile and having total fluxes similar to those of our ETG sample. The simulated galaxies were placed in empty sky regions of the COSMOS ACS image, close to our real galaxies (within ∼1 arcmin), resulting in similar values of background noise. The noise and PSF images were constructed as for the real observed galaxies, and we tested that the results were not substantially altered if we used different PSF stars for creating and fitting the simulated galaxies.

In the two panels of Fig. 5, the local average R_e–$M*$ and n–R_e relations and their 1σ dispersion are compared with R_e, n and masses of our 12 ETGs, along with those obtained for 24 simulated objects, assuming different input luminosities, namely $m_{814,in} = 22$, 23, 23.5 and positions on the frame.

It is worth emphasizing that all the 24 simulated galaxies have the same intrinsic effective radius and the Sérsic index (i.e. we are neglecting here intrinsic size and n scatter), and yet their output $R_{e,out}$ and n_{out} well reproduce the large scatter in R_e and n observed for our real sample. The spread in size for the simulated galaxies is a result of the spread in luminosity and of the different local background noise realizations, with a tendency to underestimate the size by up to a factor of ∼3 for the faintest objects, with $m_{814,in} =$ 23–23.5. This suggests that the apparent compactness of the three smallest objects (that are also among the faintest ones) may be just a consequence of their lower S/N, but intrinsically they could not be exceptionally small in size compared to local ETGs of the same mass. Thus, within our sample of 12 very high mass ETGs at $<z_{phot}> \sim 1.6$, we do not find convincing evidence for the *small size syndrome* affecting other samples of high-z ETGs. We conclude that the sample of 12 ETGs at $z > 1.4$ shows a distribution of sizes that is fully consistent with those of local $z = 0$ ETGs of the same mass.

In order to understand these results and place them in the contest of previous findings, we run a more general suite of simulations. We built 1200 synthetic galaxies with a much wider range of parameters: $R_e = 0.2$, 0.4, 0.8, 1.6 and 3.2 arcsec (corresponding to ∼2–30 kpc

[2] http://www.stsci.edu/software/tinytim/tinytim.pdf

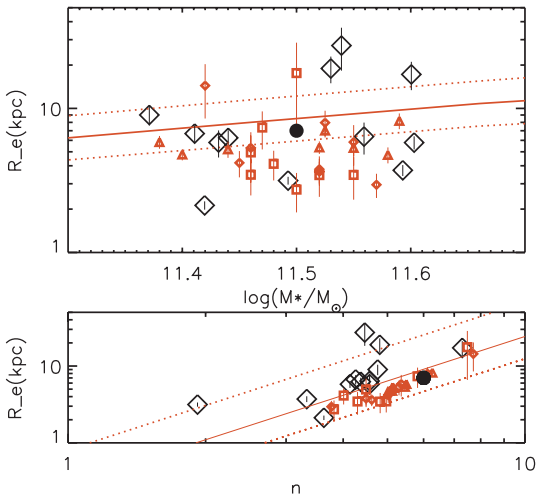

Figure 5. In the top panel, the stellar mass–size relation for our final sample of 12 ETGs (big open diamonds) is compared with the results obtained for 24 simulated objects (filled red symbols), all characterized by input Sérsic parameters of $n_{\rm in} = 6$, $R_{\rm e,in} \sim 7$ kpc and magnitude $m_{814,\rm in} = 22$ (red triangles), 23 (red diamonds) or 23.5 (red squares). The bottom panel shows the Sérsic index (n)–effective radius ($R_{\rm e}$) relation. The symbols are the same as of the top panel. In both of the diagrams, the local M*–$R_{\rm e}$ and n–$R_{\rm e}$ relations with their 1σ dispersions, from Shen et al. (2003) and Caon et al. (1993), respectively, are represented as red solid and dashed lines. The black filled circle shows the input n and $R_{\rm e}$ values common to all the 24 simulated objects. Note the large scatter in measured effective radius and the Sérsic index for the simulated objects, well reproducing the scatter observed for the real galaxies.

at $z \sim 1.5$); $n = 2$, 4, 6 and 8 and $m_{814} = 20.5$, 21, 22, 23 and 23.5. In particular, since the ACS/F814W magnitudes of the galaxies in our sample are in the range $m_{814} \sim 22$– 23.5, this allowed us to explore the size-estimate dependence on the S/N over a range of S/N $\simeq$ 50–200 (here as well as below we refer to the galaxy S/N as measured within a 1 arcsec diameter aperture).

These simulations show that the size estimates are affected by a combination of three factors: (i) the S/N of the galaxy image, (ii) the intrinsic galaxy size ($R_{\rm e}$) and (iii) the profile shape (n). The effects of these three factors are discussed below.

(i) As expected, the brighter the simulated objects, i.e. the higher the S/N, the better the accuracy in the recovered parameters. As illustrated in Fig. 6, the fainter the input magnitude, the smaller the recovered effective radius, i.e. the stronger the underestimate of the size.

(ii) For simulated galaxies with parameters and S/N similar to those of our 12 real ETGs ($m_{814} \simeq 22$– 23.5), the mean difference between the input and output effective radii turns out to be $<\Delta R_{\rm e}/R_{\rm e}> = <(R_{\rm e,in} - R_{\rm e,out})/R_{\rm e,in}> \simeq 0.15$, with a dispersion of $\sigma(\Delta R_{\rm e}/R_{\rm e}) \sim 0.46$, with most of this systematic offset and large dispersion being due to the largest simulated objects. For $R_{\rm e,in} <$ 0.8 arcsec the average offset is very close to zero, with a small scatter. Beyond $R_{\rm e,in} = 0.8$ arcsec we found that the output $R_{\rm e}$ underestimates the input radius and the scatter increases.

(iii) The size estimates depend on the capability of recovering the Sérsic index, since the best-fitting parameters are correlated via the n– $R_{\rm e}$ and n–$M*$ relations (Caon, Capaccioli & D'Onofrio 1993; D'Onofrio, Capaccioli & Caon 1994). Thus, for input $n > 4$, the output n values tend to be underestimated up by a factor of $\sim$1.5, and mostly for galaxies with the lowest S/N. Hence, this underestimate of n is accompanied by a size underestimate, as illustrated in Fig. 6.

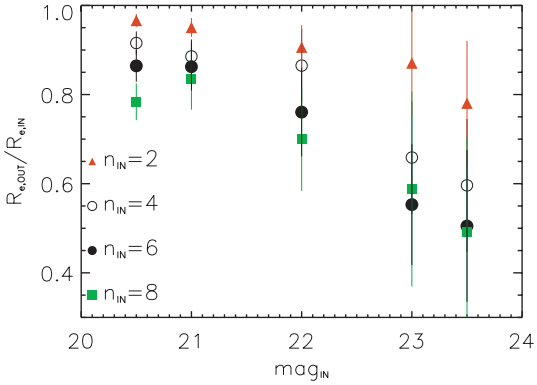

Figure 6. Simulated galaxies. $R_{\rm e,out}/R_{\rm e,in}$ (kpc) as a function of input magnitude ($m_{814,\rm in} = 20.5$, 21, 22, 23, 23.5), for a fixed large value of effective radius, i.e. $R_{\rm e,in} \sim 0.8$ arcsec, corresponding to $R_{\rm e,in} \sim 7$ kpc at $z \sim 1.5$, and different values of input Sérsic index, as labelled in the diagram. Worth noting that the $R_{\rm e,out}$ estimate decreases with decreasing luminosity and increasing Sérsic index of the source.

The recovered effective radius decreases with increasing n index (and decreasing luminosity). Similar trends are generally found for simulated galaxies with $R_{\rm e,in} \gtrsim 3.5$ kpc.

These experiments confirm that for objects with large effective radius and Sérsic index, as ETGs with masses of $> 2.5 \times 10^{11}$ M$_\odot$ are expected to be, with the typical S/N of our 12 ETGs (i.e. S/N$\leq$50–100) one could still substantially underestimate n and $R_{\rm e}$. This may be due to the fact that the haloes in high Sérsic index profiles are very extended and therefore have very low surface brightness, so that they can be easily missed in the noise at high redshift given that the surface brightness scales as $(1 + z)^4$.

A remarkable exemplification of this situation is shown in Fig. 7 for the galaxy 136738, the most massive and K-band brightest ETG in our sample. A giant low surface brightness halo is clearly detected, extending over some 4 arcsec in diameter around the galaxy (about 34 proper kpc at $z = 1.5$), at a typical level of the order of 26 mag arcsec^{-2}. Given the faintness of this structure, it would be obviously very easy to miss in the noise similar haloes at a lower S/N.

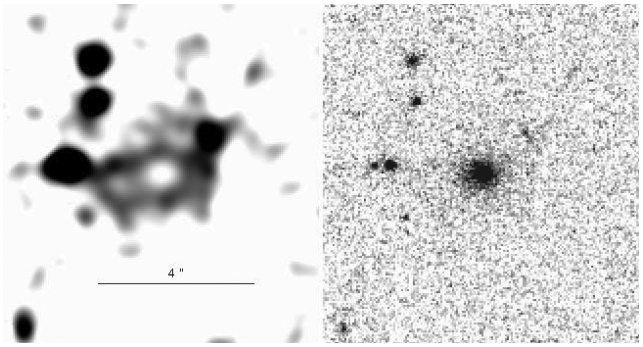

Figure 7. Left-hand panel: the ACS I-band image of #136738 (see also Fig. 2), the most massive and K-band brightest ETG in our sample. We have masked the central bright core and convolved the image with an FWHM = 0.5 arcsec Gaussian kernel in order to enhance low surface brightness details. A very extended low surface brightness halo is clearly detected, surrounding the galaxy. Right-hand panel: the original ACS I-band image without smoothing.

4 DISCUSSION AND CONCLUSIONS

Over the 2 deg^2 COSMOS field, we have identified and studied the 12 K-band brightest and most massive ($M > 2.5 \times 10^{11}$ M$_\odot$) ETGs at $z \gtrsim 1.4$. Out of them, nine follow the same size–mass relation of local ellipticals, and three appear to have smaller effective radii. However, our simulations show that their effective radius may have been underestimated by a factor of 2–3 because of their lower S/N. Hence, for the whole sample we find no compelling evidence of departures from the local size–mass relation.

Most previous studies of high-z ETGs were restricted to much smaller areas, hence they may have missed the brightest/largest ETGs similar to those reported here, as their surface number density is very low, i.e. $\sim 6.3 \pm 1.8$ deg^{-2} to the limiting magnitude of the present sample. Using the redshift range $1.4 < z < 1.8$ to estimate the cosmological volume, this corresponds to a space density of $1.4 \pm 0.4 \times 10^{-6}$ Mpc^{-3}. This is roughly 10 per cent of the space density of local ETGs selected with $M > 2.5 \times 10^{11}$ M$_\odot$. It is not clear if the different results of the present work compared to previous studies of high-z ETGs are due to the galaxies in our sample being much more massive than those in most previous works. Combining the results of our 12 massive ETGs with the literature results – so to span a wide range of masses (2 dex) – we note that the departure of ETGs at $1.4 \leq z \leq 2$ from the $z = 0$ size–mass relation seems to be differential with mass, with $R_e(z = 0)/R_e(z)$ being on average close to 1 for the most massive systems, and $\sim$2–4 for lower masses. This is reminiscent of the general downsizing scenario, whereby massive ETGs formed their stars and assembled their mass more rapidly and at higher redshifts compared to the less massive ones. Thus, the present results may extend the downsizing effect to the internal structure of ETGs, with the most massive ETGs reaching their internal and dynamical structure earlier and faster than lower mass ETGs at the same redshift.

However, we also argue that bias in the galaxy-profile fitting could significantly affect the size measurements, as low surface brightness haloes could remain undetected in high-redshift ellipticals if observed with low S/N (e.g. Fig. 7). Based on redshifted mock images of local systems, Hopkins et al. (2009) also concluded that there is a tendency to underestimate the galaxy size which is more pronounced in the most massive galaxies, due to their large R_e and n. This is in agreement with the results of our simulations. They also stressed that elliptical galaxy profiles are not perfectly 'Sérsic', which would contribute to the size underestimate at high redshift.

Thanks to the exceptional brightness of our 12 ETGs, their S/N in the single-orbit COSMOS I-band images are among the highest reached by *HST*+ACS imaging of high-z ETGs, and are comparable to those obtained by D05 for *pBzK*s in the extremely deep HUDF images. On average, their S/N is also nearly three times higher than that of galaxies in the Galaxy Mass Assembly Ultra-deep Spectroscopic Survey (GMASS) study, which used Great Observatory Origins Deep Survey – South (GOODS-S) z-band data (Cimatti et al. 2008). Hence, it is also possible that in these studies the effect of the noise has led to underestimate the size of some object by a factor of 2 or 3. Cimatti et al. (2008) used simulated objects to check the reliability of their derived effective radii, and estimated an average scatter on the galaxy size measurements of $\sim$20 per cent, with no strong bias. This suggests that a size underestimate is unlikely to account for the small size obtained for the bulk of the GMASS high-z ETGs. Still, the parameter space (n, R_e, S/N) explored in the simulations of Cimatti et al. (2008) may not fully include that occupied by the real GMASS galaxies, hence we cannot exclude that in this study the size of some of the intrinsically largest galaxies may have been underestimated by more than 20 per cent.

On the other hand, some studies using H-band (F160W) Near Infrared Camera and Multi-Object Spectrometer (NICMOS)-2 imaging (e.g. Longhetti et al. 2007; van Dokkum et al. 2008) have also reached high S/N, thanks to them sampling longer rest-frame wavelengths where the flux of ETGs is much stronger than in the near-ultraviolet. Using the NICMOS exposure time calculator, we estimated that the S/N of galaxies in Longhetti et al. (2007) and van Dokkum et al. (2008) were on average quite comparable, or sometimes even slightly higher than the ones obtained for our COSMOS ETG sample. The masses of ETGs in the former study (open triangles in Fig. 4) are similar to those of our galaxies, and yet the derived effective radii are up to three times smaller than those of local ellipticals with similar masses. Based on simulations, the authors argued that their typical image resolution and S/N led to underestimate by $\sim$25 per cent the effective radii of galaxies with an intrinsic $n = 4$ and radii in the range of $\sim$1–4 kpc, and took into account this result in their galaxy size estimate. However, they did not verify the robustness of their fitting procedure in recovering the light profiles of galaxies with $R_e > 4$ kpc and $n > 4$, typical of such extremely massive ETGs ($M > 2.5 \times 10^{11}$ M$_\odot$), which we found instead to be affected by a substantial bias.

Similarly, van Dokkum et al. (2008) found their ETGs nearly five times smaller compared to local ETGs of similar mass. However, their stellar masses were estimated using the stellar population models of Bruzual & Charlot (2003) that do not include stars in their thermally pulsing asymptotic giant branch (TP-AGB) phase, and therefore stellar masses of ETGs at $z \gtrsim 1.4$ might have been overestimated by a factor of $\sim$1.5–2 (Maraston et al. 2006), while the TP-AGB effect is negligible for local ETGs. In the size–mass diagram, this mass rescaling would reduce by nearly three times the average offset in size with respect to the local relation (as shown in Fig. 4). Moreover, allowing for a systematic underestimate of the size of the galaxies with lower S/N, similar to the one found by Longhetti et al. (2007) for lower redshift ETGs in NIC2 images, we conclude that some galaxy in the study of van Dokkum et al. (2008) may actually follow the local size–mass relation.

Saracco et al. (2009) collected 32 high-redshift ETGs with archival NICMOS data, among which 13 have given size comparable to the local galaxies and the others are more than 1σ smaller compared to the local relation. Also in this case, based on the above arguments, we cannot exclude that the size of the galaxies with lower S/N and lower resolution (those observed only with NICMOS-3) may have been underestimated. However, the authors suggested an age-dependent evolution, with the *young* ETGs (mean stellar age $<$2 Gyr) being more similar to their local counterparts and the *old* ETGs being denser. Our results cannot confirm such claim, as our best-fitting ages are all confined within a very narrow range (see Table 1).

A potentially powerful test of the reliability of the size estimates of high-z ETGs consists in measuring their velocity dispersion $\sigma_\star$, which would allow us to check for the consistency of the three quantities entering the virial relation: $M_{dyn} \simeq 5 \times R_e\, \sigma_\star^2/G$, with the constraint of the stellar mass being less than the dynamical mass. Due to the limits of the present-day telescopes, the low S/N of the available spectra of ETGs at $z > 1.4$ allowed only a few attempts in this direction, most of which based on the analysis of average stacked spectra of several objects (Cenarro & Trujillo 2009; Cappellari et al. 2009). These two studies, both based on the GMASS sample of spectra (Cimatti et al. 2008), found that

the resulting stellar and dynamical masses appear to be consistent with each other within the errors. However, Cappellari et al. (2009) found a trend to underestimate the virial masses ($M_{\rm dyn}$) on average by ∼30 per cent, that may be ascribed to a size underestimate by a similar quantity. Thanks to a >7 S/N of their spectra, Cappellari et al. also measured the $\sigma_\star$ from the individual spectra of two of the galaxies with the largest size in the GMASS sample (whose sizes are consistent with those of local ETGs). The resulting agreement with the masses and sizes previously estimated by Cimatti et al. (2008) confirmed that these two objects are truly similar to local ETGs, as most of the ETGs in our sample. Most recently, van Dokkum, Kriek & Franx (2009) analysed the near-IR spectrum of an ETG at $z = 2.2$ finding a very high velocity dispersion ($\sigma_\star \sim 510$ km s^{-1}), consistent with the small size measured for this object, which then suggests a strong structural/dynamical evolution from $z \sim 2$ to 0 for similarly massive ETGs. Yet, the relatively low S/N of the near-IR spectrum implies a fairly large uncertainty in the measured $\sigma_\star$. Recently, some among us were able to obtain a good S/N near-IR spectrum of one of our 12 ETGs (object 254025) with the Multi-Object Infrared Camera and Spectrograph (MOIRCS) spectrograph at the Subaru telescope, and a measurement of $\sigma_\star$ will be attempted (M. Onodera et al. in preparation).

We conclude that the fraction of high-redshift ETGs which are genuinely undersized with respect to local ETGs is still poorly known. Several massive ETGs at high redshift (certainly the majority in our sample) are as large as their local counterparts, and therefore recipes aimed at inflating putative small ETGs should avoid to create oversize ETGs at low redshifts out of those having already reached their final size at $z \gtrsim 1.4$. We also hint at a possible downsizing effect not only on stellar ages and mass assembly but also on the structural properties of these galaxies, with the most massive ETGs being in all respects the first to reach their final configuration.

ACKNOWLEDGMENTS

We wish to thank Swara Ravindranath and Paolo Cassata for useful discussions. This work has been supported by grants ASI/COFIS/WP3110+WP3400 I/026/07/0. CM, ED, FS, HJM and MO acknowledge funding support of French ANR under contracts ANR-07-BLAN-0228 and ANR-08-JCJC-0008, and CM thanks CEA Saclay for hospitality and funding at the beginning of this work.

REFERENCES

Bernardi M., 2009, MNRAS, 395, 1491
Bertin E., Arnouts S., 1996, A&AS, 117, 393
Bolzonella M., Miralles J.-M., Pelló R., 2000, A&A, 363, 476
Bruzual G., Charlot S., 2003, MNRAS, 344, 1000
Buitrago F., Trujillo I., Conselice C. J., Bouwens R. J., Dickinson M., Yan H., 2008, ApJ, 687, L61
Caon N., Capaccioli M., D'Onofrio M., 1993, MNRAS, 265, 1013
Cappellari M. et al., 2009, ApJ, 704, L34
Cenarro A. J., Trujillo I., 2009, ApJ, 696, L43
Chabrier G., 2003, PASP, 115, 763
Chary R., Elbaz D., 2001, ApJ, 556, 562
Cimatti A. et al., 2004, Nat, 430, 184
Cimatti A. et al., 2008, A&A, 482, 21
Daddi E. et al., 2004, ApJ, 600, L127
Daddi E. et al., 2005, ApJ, 626, 680 (D05)
Daddi E. et al., 2007, ApJ, 670, 156
Damjanov I. et al., 2009, ApJ, 695, 101
D'Onofrio M., Capaccioli M., Caon N., 1994, MNRAS, 271, 523
Fan L., Lapi A., De Zotti G., Danese L., 2008, ApJ, 689, L101
Glazebrook K. et al., 2004, Nat, 430, 181
Hopkins P. F., Bundy K., Murray N., Quataert E., Lauer T., Ma C.-P., 2009, MNRAS, 398, 898
Ilbert O. et al., 2009, ApJ, 690, 1236
Khochfar S., Silk J., 2006, ApJ, 648, L21
Koekemoer A. M. et al., 2007, ApJS, 172, 196
Krist J., Hook R., 2004, The TINY TIM User's Guide. Available online www.stsci.edu/software/tinytim/tinytim.pdf
La Barbera F., de Carvalho R. R., 2009, ApJ, 699, 76L
Le Floc'h E. et al., 2009, ApJ, 703, 222
Lejeune T., Cuisinier F., Buser R., 1997, A&AS, 125, 229
Longhetti M. et al., 2007, MNRAS, 374, 614
Maraston C., 2005, MNRAS, 362, 799
Maier C. et al., 2009, ApJ, 694, 1099
McCracken H. J. et al., 2009, ApJ, submitted (arXiv:0910.2705)
McGrath E. J., Stockton A., Canalizo G., Iye M., Maihara T., 2008, ApJ, 682, 303
Maraston C., Daddi E., Renzini A., Cimatti A., Dickinson M., Papovich C., Pasquali A., Pirzkal N., 2006, ApJ, 652, 85
Naab T., Johansson P. H., Ostriker J. P., Efstathiou G., 2007, ApJ, 658, 710
Pannella M., Gabasch A., Goranova Y., 2009, ApJ, 701, 787
Peng C. Y., Ho L. C., Impey C. D., Rix H.-W., 2002, AJ, 124, 266
Rettura A., Rosati P., Nonino M., 2009, in Giobbi G., Tornambe A., Raimondo G., Limongi M., Antonelli L. A., Menci N., Brocato E., eds, AIP Conf. Proc. Vol. 1111, Probing Stellar Populations Out to the Distant Universe: Cefalu 2008. Am. Inst. Phys., Melville, p. 183
Sanders D. B. et al., 2007, ApJS, 172, 86
Saracco P., Longhetti M., Andreon S., 2009, MNRAS, 392, 718
Sérsic J. L., 1968, Atlas de galaxias australes. Observatorio Astronomico, Cordoba, Argentina
Shen S., Mo H. J., White S. D. M., Blanton M. R., Kauffmann G., Voges W., Brinkmann J., Csabai I., 2003, MNRAS, 343, 978
Tacconi L. J. et al., 2008, ApJ, 680, 246
Taylor E. N. et al., 2009, ApJ, submitted (arXiv:0907.4766)
Toft S. et al., 2007, ApJ, 671, 285
Trujillo I. et al., 2006, ApJ, 650, 18
Trujillo I., Conselice C. J., Bundy K., Cooper M. C., Eisenhardt P., Ellis R. S., 2007, MNRAS, 382, 109
Trujillo I., Cenarro A. J., de Lorenzo-Cáceres A., Vazdekis A., de la Rosa I. G., Cava A., 2009, ApJ, 692, L118
Valentinuzzi T. et al., 2009, ApJ, submitted (arXiv:0907.2392)
van der Wel A., Holden B. P., Zirm A. W., Franx M., Rettura A., Illingworth G. D., Ford H. C., 2008, ApJ, 688, 48
van Dokkum P. G. et al., 2008, ApJ, 677, L5
van Dokkum P. G., Kriek M., Franx M., 2009, Nat, 460, 717
Zirm A. W. et al., 2007, ApJ, 656, 66

This paper has been typeset from a TEX/LATEX file prepared by the author.